Cell

Persistent Telomere Damage Induces Bypass of Mitosis and Tetraploidy

Teresa Davoli,[1] Eros Lazzerini Denchi,[1,2] and Titia de Lange[1,*]
[1]Laboratory for Cell Biology and Genetics, The Rockefeller University, 1230 York Avenue, New York, NY 10065, USA
[2]Present address: Department of Genetics, The Scripps Research Institute, 3040 Science Park Road, La Jolla, CA 92121, USA
*Correspondence: delange@mail.rockefeller.edu
DOI 10.1016/j.cell.2010.01.031

SUMMARY

Tetraploidization has been proposed as an intermediate step toward aneuploidy in human cancer but a general mechanism for the induction of tetraploidy during tumorigenesis is lacking. We report that tetraploidization occurs in p53-deficient cells experiencing a prolonged DNA damage signal due to persistent telomere dysfunction. Live-cell imaging revealed that these cells have an extended G2 due to ATM/ATR- and Chk1/Chk2-mediated inhibition of Cdk1/CyclinB and eventually bypass mitosis. Despite their lack of mitosis, the cells showed APC/Cdh1-dependent degradation of the replication inhibitor geminin, followed by accumulation of Cdt1, which is required for origin licensing. Cells then entered a second S phase resulting in whole-genome reduplication and tetraploidy. Upon restoration of telomere protection, these tetraploid cells resumed cell division cycles and proliferated. These observations suggest a general mechanism for the induction of tetraploidization in the early stages of tumorigenesis when telomere dysfunction can result from excessive telomere shortening.

INTRODUCTION

Aneuploidy is a hallmark of solid human cancers. Diploid cells can acquire an aneuploid chromosome complement through repeated chromosome nondisjunction events (reviewed in Kops et al., 2005). However, as many solid tumors have subtetraploid karyotypes and supernumerary centrosomes, it is likely that the initial step toward aneuploidy is tetraploidization (reviewed in Storchova and Kuffer, 2008). Tetraploid cells, most likely because they can form multipolar spindles, have a high rate of chromosome missegregation, explaining how tumors attain subtetraploid karyotypes in which some chromosomes are present at four copies whereas other chromosomes have a lower copy number. Tetraploidization has been observed in the early stages of colon cancer (Danes, 1978; Levine et al., 1991), Barrett's esophagus (Galipeau et al., 1996; Rabinovitch et al., 1989), breast cancer (Dutrillaux et al., 1991), and cervical cancer (Olaharski et al., 2006). Three main mechanisms for tetraploidization in the context of human cancer have been proposed: cell fusion, a failure to complete mitosis (mitotic slippage), and a failure to complete cytokinesis (reviewed in Ganem et al., 2007).

Here, we show that tetraploidization can occur in response to the loss of telomere protection, which is thought to be a common event in human tumorigenesis (reviewed in Maser and DePinho, 2002). The telomeres of most human somatic cells undergo progressive telomere shortening due to the repression of telomerase. This process eventually limits cellular proliferation through the induction of apoptosis or senescence and is thought to represent a tumor-suppressor mechanism that can be subverted by the activation of telomerase (Kim et al., 1994; Bodnar et al., 1998). In agreement, extreme telomere shortening is observed in the early stages of tumorigenesis before telomerase is activated (Chin et al., 2004). Furthermore, most clinically relevant human tumors, including telomerase-positive tumors, have short telomeres that bear witness to the telomere shortening in their proliferative history (de Lange et al., 1990; Hastie et al., 1990). Thus, many human cancers might experience an episode of diminished chromosome-end protection during their development.

Telomeres that have become dysfunctional after extensive shortening activate the canonical DNA damage signaling pathways, mediated by the ATM and ATR kinases (d'Adda di Fagagna et al., 2003). At functional telomeres, ATM signaling is repressed by the shelterin component TRF2, whereas the single-stranded telomeric DNA-binding protein POT1 blocks the activation of the ATR kinase (Denchi and de Lange, 2007). In the current study, telomere dysfunction is experimentally induced in mouse embryo fibroblasts (MEFs) that contain floxed alleles of the two mouse POT1 genes, POT1a and POT1b (Hockemeyer et al., 2006). Depletion of POT1a/b induces an ATR kinase response that leads to accumulation of DNA damage factors at chromosome ends and activation of the effector kinases Chk1 and Chk2 (Denchi and de Lange, 2007). This DNA damage response is persistent because the repair of the damaged telomeres by NHEJ is repressed by TRF2, which remains associated with telomeres despite the removal of POT1a and -b (Hockemeyer et al., 2006).

When POT1a/b are deleted from MEFs that lack a functional p53 pathway, the cells undergo polyploidization, resulting in

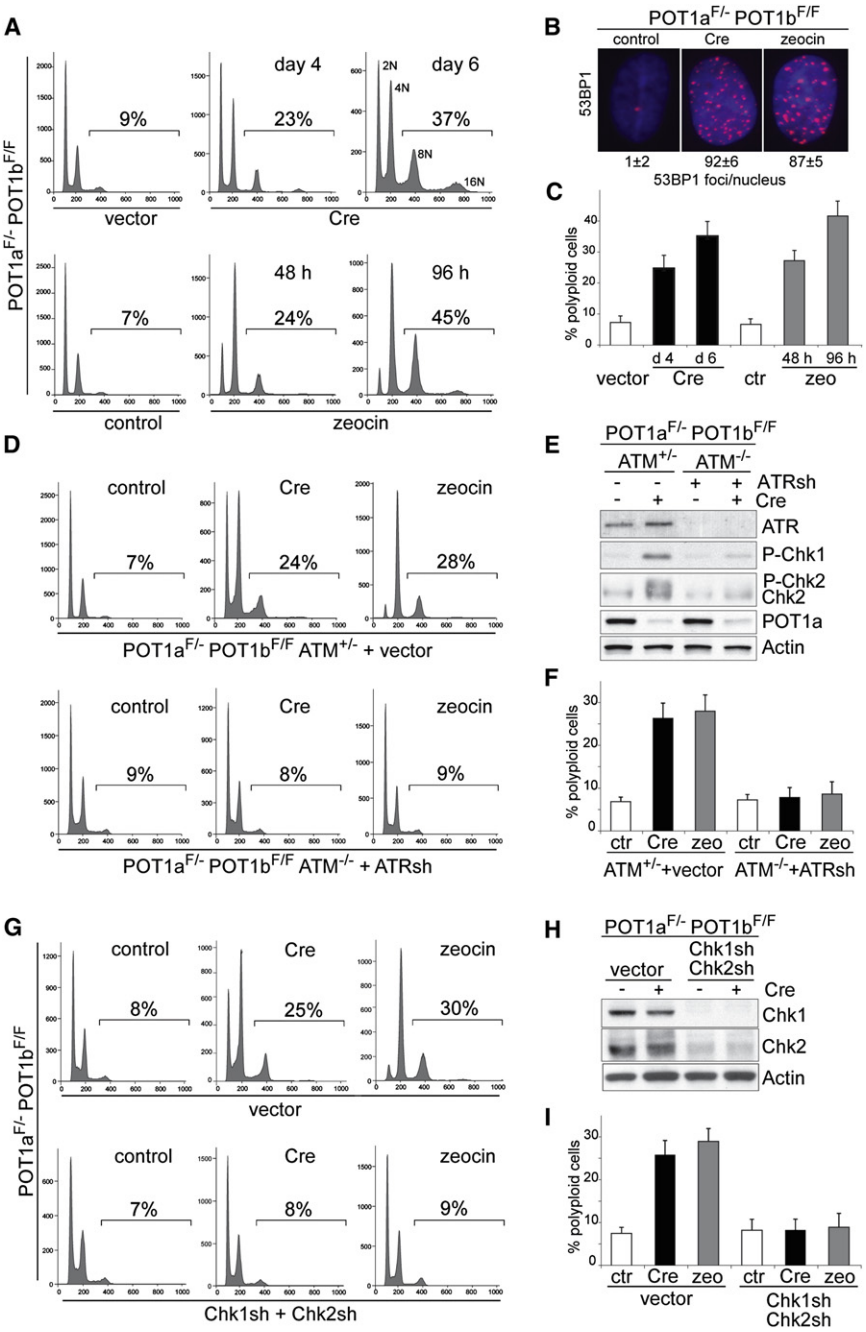

Figure 1. Polyploidy Induced by Persistent DNA Damage Signaling

(A) Polyploidization upon deletion of POT1a/b or continuous zeocin treatment. POT1a$^{F/-}$POT1b$^{F/F}$ MEFs were treated with Cre, the vector control, zeocin, or left untreated and analyzed by FACS at the indicated time points The percentage of cells with DNA content > 4n is given. Representative FACS analyses are shown. See also related Figure S1A.

(B) 53BP1 foci in POT1a/b DKO cells and zeocin-treated cells. POT1a$^{F/-}$POT1b$^{F/F}$ MEFs were treated with Cre, zeocin, or left untreated as in (A) and processed for IF for 53BP1 (red) (DNA stained with DAPI [blue]). Average 53BP1 foci/nucleus and SEMs are given (n > 50).

(C) Quantification of polyploidy induced by POT1a/b deletion or continuous zeocin. POT1a$^{F/-}$POT1b$^{F/F}$ MEFs were treated and analyzed as in (A). The bars show the average values and SDs of three independent experiments.

(D–F) Diminished polyploidy after inhibition of ATM and ATR. POT1a$^{F/-}$POT1b$^{F/F}$ATM$^{-/-}$ and POT1a$^{F/-}$POT1b$^{F/F}$ATM$^{+/-}$ were treated with ATR shRNA or vector control. Polyploidy was measured as in (A). FACS profiles from a representative experiment (D) and quantification of the percentage of polyploid cells in three independent experiments with SDs (F) are shown. Immunoblotting showing ATR knockdown and phosphorylation of Chk1 and Chk2 in the indicated cells is shown in (E). See also related Figures S1C–S1E.

(G–I) Diminished polyploidy after impairment of Chk1 and Chk2. POT1a$^{F/-}$POT1b$^{F/F}$ MEFs were treated with Chk1 and Chk2 shRNAs (set 1) or vector control. Polyploidy was measured as in (D). FACS profiles from a representative experiment (G) and quantification of the percentage of polyploid cells in three independent experiments with SD (I) are shown. Immunoblotting showing Chk1 and Chk2 knockdown is in (H). See also related Figures S1F and S1G.

RESULTS

Polyploidization Induced by Persistent DNA Damage Signaling

The two mouse POT1 proteins were removed from telomeres through Cre-mediated gene deletion in POT1a$^{F/-}$POT1b$^{F/F}$MEFs, resulting in POT1a/b double knockout (DKO) cells. These and other cells used in this study are permissive for polyploidization because p53, which can block entry into S phase in tetraploid cells (Carder et al., 1993; Andreassen et al., 2001), is repressed by SV40 Large T antigen (SV40LT). As expected, POT1a/b DKO cells showed a DNA damage response and polyploidization characterized by FACS profiles with discrete 8n and 16n peaks (Figures 1A–1C and Figure S1A available online). The polyploid cell fraction (defined here as the fraction of cells with a DNA content >4n) increases from a basal level of 7% to 8% to 35% to 40% at day 6 after POT1a/b deletion 4n, 8n, and 16n DNA content (Hockemeyer et al., 2006). The FACS profile of these cultures shows discrete peaks suggesting that the whole genome is duplicated. Furthermore, the occasional metaphase spreads obtained from POT1a/b DKO cultures show diplo- and quadruplochromosomes indicating that these cells have undergone two or three rounds of DNA replication without resolution of the centromeric cohesin. Here, we document the consequences of telomere dysfunction in this setting and demonstrate that bypass of mitosis and endoreduplication are induced by the persistent DNA damage signal emanating from permanently damaged telomeres.

(Figures 1A and 1C) and the cells accumulated supernumerary centrosomes (Figure S1B). To determine whether this polyploidization was due to a DNA damage signal, we generated SV40LT-immortalized POT1a$^{F/-}$POT1b$^{F/F}$ATM$^{-/-}$ MEFs and treated the cells with an shRNA to ATR (Figures 1D–1F). Littermate-derived, SV40LT-immortalized POT1a$^{F/-}$POT1b$^{F/F}$ATM$^{+/-}$ MEFs infected with the shRNA vector served as a control. Inhibition of ATM and ATR diminished the phosphorylation of Chk1 and Chk2 and decreased the induction of polyploidy in response to POT1a/b deletion (Figures 1D–1F). Consistent with the ATR kinase being primarily responsible for the DNA damage signal in POT1a/b DKO cells, inhibition of ATR alone strongly reduced the fraction of polyploid cells (Figures S1C and S1D). ATR knockdown did not affect DNA replication per se (Figure S1E). Polyploidization was also diminished by knockdown of Chk1 and Chk2 (Figures 1G–1I) or treatment with UCN01 (Figures S1F and S1G). These data establish that a DNA-damage signaling cascade involving ATM/ATR and Chk1/Chk2 is required for polyploidization in response to telomere dysfunction.

The telomere damage in the POT1a/b DKO cells is not efficiently repaired and therefore elicits a DNA damage signal that persists. A persistent DNA damage signal due to unrepaired telomere damage also occurs when TRF2 is deleted from Lig4$^{-/-}$ (NHEJ-deficient) cells (Celli and de Lange, 2005). Consistent with the data on POT1a/b DKO cells, the Lig4/TRF2-deficient cells showed polyploidization and diplochromosomes, although the magnitude of the phenotype was less (Figures S1H and S1I).

To further test the idea that polyploidization occurs when a DNA damage signal persists, we monitored the effects of continuous treatment with the DSB-inducing agent, zeocin. The zeocin concentration used induced the same level of DNA damage as deletion of POT1a/b (Figure 1B). Cells treated with zeocin showed a polyploid FACS profile characterized by discrete 8n and 16n peaks (Figures 1A and 1C). Zeocin-mediated induction of polyploidy was strongly impaired when either ATR/ATM or Chk1/Chk2 were inhibited (Figures 1D–1I). The absence of ATM, which transduces the initial response to the DSBs, had a stronger effect than knockdown of ATR (Figures S1C and S1D).

Polyploidy was also induced by continuous treatment with doxorubicin or bleomycin, and by repeated UV irradiation (Figures S1J–S1L). Moreover, tetraploidization was induced by overexpression of the ATR-activating domain of TopBP1 (Figure S1J). Since this TopBP1 domain has been shown to activate ATR in the absence of DNA lesions (Toledo et al., 2008), this result argues that DNA damage signaling rather than the DNA lesions themselves causes polyploidization.

DNA damage-induced polyploidization was not a peculiarity of mouse cells, as prolonged zeocin treatment of HPV-E6/E7-transformed human BJ fibroblasts also resulted in tetraploidy (Figures S1M and S1N). Furthermore, the polyploidization was not due to the expression of viral oncoproteins since it occurred in zeocin-treated p53$^{-/-}$ MEFs (Figure S1O) and in TRF2$^{-/-}$Lig4$^{-/-}$p53$^{-/-}$ MEFs (Figure S1I). In contrast, primary MEFs and BJ fibroblasts with an intact p53 pathway showed the expected G1/S arrest in response to DNA damage (data not shown).

Lack of Cdk1/CyclinB Activation and Stabilization of APC/Cdc20 Targets

Metaphase spreads from POT1a/b DKO cells show diplo- and quadruplochromosomes, indicating that the cells undergo two rounds of whole genome duplication without intervening destruction of the centromeric cohesin. Cohesin is normally degraded when the APC/Cdc20 ubiquitin ligase is activated at the onset of anaphase. We therefore monitored the status of mitotic targets of the APC/Cdc20 in synchronized POT1a/b DKO cells (Figure 2A). Upon release from a G1/S block, both control and POT1a/b DKO cells entered S phase, as shown by BrdU incorporation. However, POT1a/b DKO cells progressed into S-phase somewhat slower (Figure 2B) and did not divide in the 10 hr time period (Figure 2A). Each of the nine APC targets tested, including securin, which protects cohesin from degradation by separase, were abnormally stabilized in POT1a/b DKO cells (Figure 2A). In contrast, CyclinE, a target of the SCF ubiquitin ligase, was degraded with normal kinetics in POT1a/b DKO cells (Figure 2A).

We next analyzed the activity of Cdk1/CyclinB, which is required for entry into mitosis and contributes to the activation of the APC/Cdc20 (reviewed in Peters, 2002). Cdk1/CyclinB activation can be blocked by ATM/ATR kinase signaling through Chk1/Chk2-mediated inactivation of the Cdc25 phosphatases, which remove inhibitory phosphates from Tyr14/15 of Cdk1. The Cdk1/CyclinB activity in synchronized POT1a/b DKO cells was ~4-fold lower than in the control and phosphorylation of Tyr14/15 was increased (Figures 2C and 2D). Furthermore, the Cdk1/CyclinB kinase activity remained low for at least 6 days after POT1a/b deletion and during 72 hr of zeocin treatment (Figure S2A). In contrast, the Cdk2/CyclinE activity was not obviously altered (Figure 2E). Knockdown of Chk1 and Chk2 in POT1a/b DKO cells resulted in an increase in Cdk1/CyclinB activity and the phosphorylation of Tyr14/15 was diminished (Figures 2D and 2F). In addition, when Chk1 and Chk2 were inhibited with shRNAs or UCN01, the level of several APC/Cdc20 targets decreased (Figure 2D and Figure S2B), suggesting that APC/Cdc20 was more active.

Bypass of Mitosis

To further analyze the altered cell cycles, we used time-lapse live-cell imaging of asynchronously growing POT1a/b DKO cells and zeocin-treated cells. During the 2 day imaging session, a fraction of the cells became polyploid, whereas control cells divided normally and remained diploid (Figure 3A, Figure S3, and Movie S1). On average, each cell in the control cultures went through mitosis twice whereas 72% of the POT1a/b DKO cells and 86% of the zeocin-treated cells did not divide during the imaging period (Figures 3A and 3B and Movie S1). Furthermore, neither the POT1a/b DKO cells, nor the zeocin-treated cells showed nuclear envelope breakdown or chromosome condensation as deduced from H2B-GFP expressing cells (data not shown). In comparison with control cells, POT1a/b DKO and zeocin-treated cells became large and flattened, displaying a senescent-like phenotype. The POT1a/b DKO cells and zeocin-treated cells showed an ~2-fold increase in the nuclear area during the imaging period ($p < 0.001$; Figure 3C), consistent with their increased DNA content. We also monitored

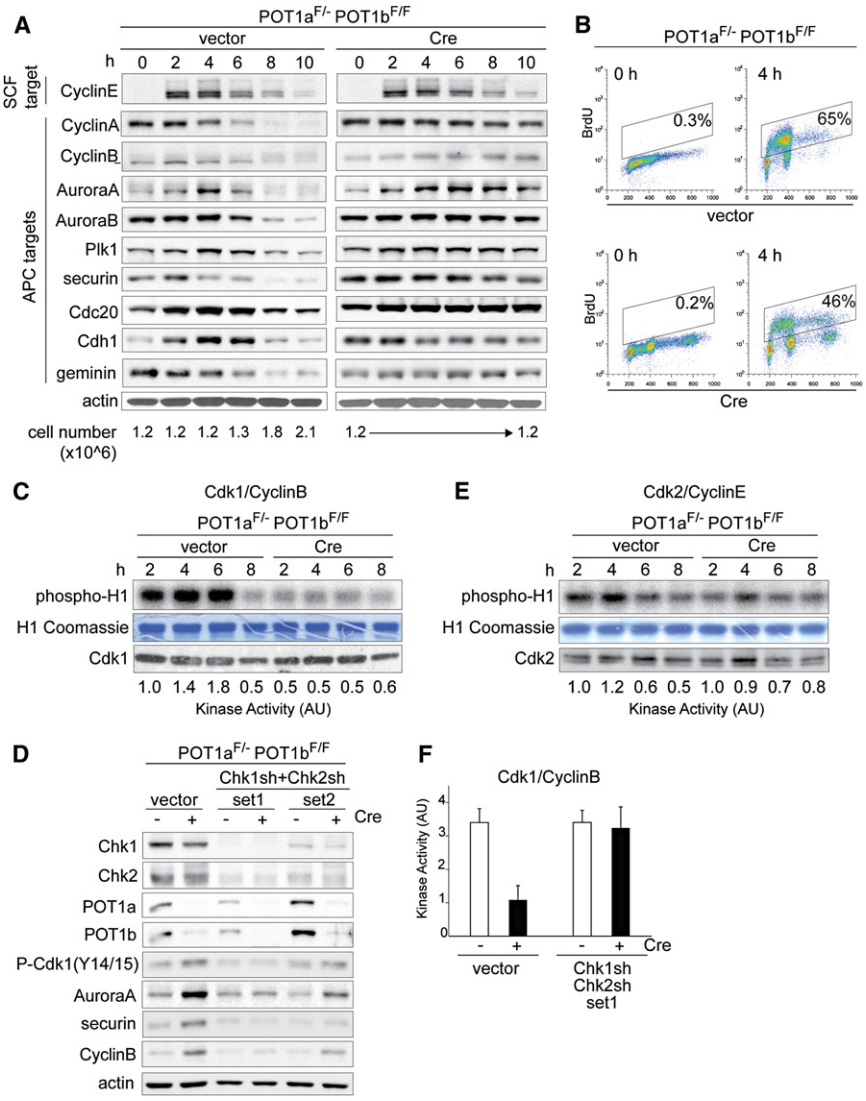

Figure 2. Impaired Activity of Cdk1/CyclinB and APC/Cdc20

(A) Abnormal stabilization of mitotic APC targets in POT1a/b DKO cells. POT1a$^{F/-}$POT1b$^{F/F}$ MEFs were treated with Cre and 2 days later synchronized in G1/S. The indicated proteins were analyzed by immunoblotting and the cell number at the corresponding time points is indicated below the blots.

(B) S phase progression of cells used in (A). FACS analysis of BrdU positive cells at 0 and 4 hr after release from double thymidine (G1/S) block.

(C and E) Reduced Cdk1/CyclinB activity in POT1a/b DKO cells. POT1a$^{F/-}$POT1b$^{F/F}$ MEFs were treated as in (A) and the activity of Cdk1/CyclinB (C) and Cdk2/CyclinE (E) complexes was measured by histone H1-kinase assay. Phospho-histone-H1, Coomassie staining of histone H1, immunoblotting showing Cdk1 (C) and Cdk2 (E) in IPs and quantification of kinase activity are shown. See also related Figure S2A.

(D and F) Impairment in Cdk1/CyclinB and APC/Cdc20 activation in POT1a/b DKO cells is dependent on Chk1 and/or Chk2. POT1a$^{F/-}$POT1b$^{F/F}$ MEFs were treated with Cre and two sets of Chk1 and Chk2 shRNAs. Immunoblotting for the indicated proteins is shown (D). Quantification of Cdk1/CyclinB kinase activity (as in [C]) after knockdown of Chk1 and Chk2 (set 1) in two independent experiments with SD is shown (F). See also related Figure S2B.

POT1a/b DKO and zeocin-treated cells expressing a CyclinE-eGFP fusion. Although the CyclinE-eGFP signals were hard to discern, ~35% of the cells showed two waves of CyclinE-eGFP without intervening mitosis over a 2 day period (Figure 3B and Movie S2).

Alternating Geminin and Cdt1 Expression without Mitosis

The ability of POT1a/b DKO cells to enter S phase without progression through mitosis was unexpected as the initiation of DNA replication requires degradation of the DNA replication inhibitor geminin (reviewed in Blow and Dutta, 2005). Geminin, an inhibitor of the replication initiation factor Cdt1, is normally degraded at the end of mitosis. Degradation of geminin allows Cdt1, which rises in G1, to license replication origins. Once DNA replication is initiated, Cdt1 is degraded by SCF. In addition, geminin rises in S/G2, thereby blocking Cdt1 from relicensing of replication origins. This alternating expression of Cdt1 and geminin ensures that cells execute only one round of DNA replication per cell division cycle, a rule that is broken by endoreduplicating cells.

To examine the fluctuations of geminin and Cdt1, we used Fluorescent Ubiquitination-based Cell Cycle Indicator (FUCCI, [Sakaue-Sawano et al., 2008]) live-cell imaging which relies on fluorescently tagged, truncated forms of geminin (green) and Cdt1 (red) that recapitulate the degradation of the endogenous proteins. Normally cycling cells are red in G1, reflecting Cdt1 expression, become yellow upon entry into S phase when geminin begins to accumulate before Cdt1 is degraded and then are green throughout S phase and G2, due to the presence of geminin. Geminin is degraded at the end of mitosis, resulting in a brief period without either marker in G1. This sequence of events was observed in control cells (Figures 4A and 4B and Movie S3). Cre-treated POT1a/b DKO cells showed a similar Cdt1-positive G1 phase, but then displayed a prolonged geminin-positive S/G2 phase (20 hr; Figures 4A and 4B). Importantly, S/G2 was followed by loss of geminin without mitosis (Figures 4A–4C and Movie S3). Cdt1 was undetectable until geminin was degraded but then increased over the next 12–14 hr, suggesting that cells returned to a G1-like state. Eventually, the POT1a/b DKO cells attained features of early S phase, expressing both geminin and Cdt1, followed by a second period of geminin expression without Cdt1 (Figures 4A and 4B and Movie S3). Thus, the endoreduplicating POT1a/b DKO cells showed a slower cell cycle but

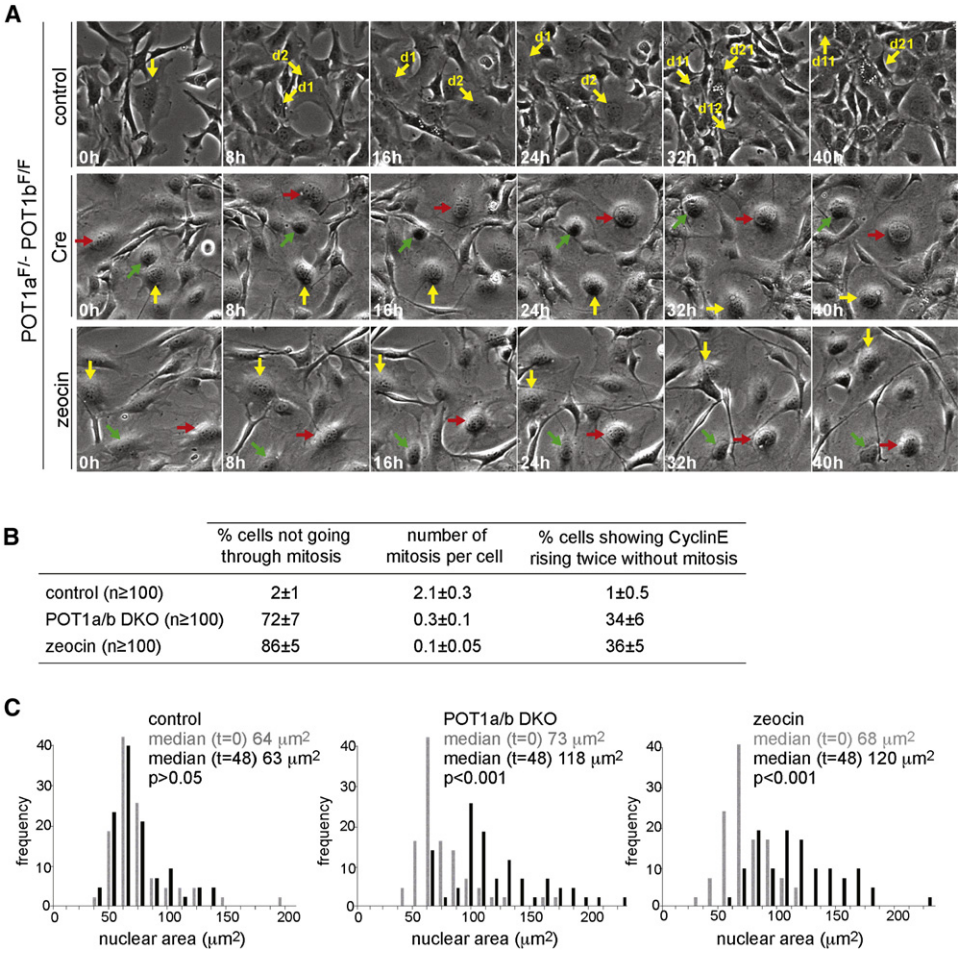

	% cells not going through mitosis	number of mitosis per cell	% cells showing CyclinE rising twice without mitosis
control (n≥100)	2±1	2.1±0.3	1±0.5
POT1a/b DKO (n≥100)	72±7	0.3±0.1	34±6
zeocin (n≥100)	86±5	0.1±0.05	36±5

Figure 3. Bypass of Mitosis in POT1a/b DKO and Zeocin-Treated Cells

(A) Time-lapse imaging of POT1a$^{F/-}$POT1b$^{F/F}$ MEFs treated with Cre, cells treated with zeocin, and the untreated controls. After 72 hr, phase-contrast microscope images were taken every 15 min for 48 hr (Movie S1). Selected time points stills are shown. Arrows of the same color highlight the same cell over the course of the imaging session. In POT1a/b DKO and zeocin-treated cells, arrows highlight representative cells not undergoing mitosis. See also related Figure S3.

(B) Quantification of cells not undergoing mitosis and the average number of mitoses per cell. Cells were treated and imaged as in (A) and the movies were analyzed. The percentage of cells showing CyclinE rising twice without an intervening mitosis in 48 hr is also shown. Cells expressing CyclinE-eGFP were analyzed as in (A) (representative movies in Movie S2). At least 100 cells in each movie were analyzed for each condition. Average values and SDs were obtained from three independent experiments.

(C) Increased nuclear area of POT1a/b DKO and zeocin-treated cells. Cells were treated and imaged as in (A). For each condition, the nuclear area of 100 cells was measured at the beginning (0 hr) and at the end (48 hr) of the imaging session and displayed as a frequency distribution. P values based on nonparametric Krustal-Wallis test. The results are representative of three independent experiments.

preserved the alternating geminin and Cdt1 expression despite the absence of mitosis. A prolonged S/G2 and mitosis-independent alternation of geminin and Cdt1 was also observed with zeocin-treated cells (Figures 4B and 4C, Figure S4A, and Movie S3). This aberrant cell-cycle pattern occurred in 70% of the POT1a/b DKO cells and 83% of zeocin-treated cells, compared to 2% of the controls (Figure 4C). In addition, FUCCI imaging showed that zeocin treatment induced mitosis-independent geminin degradation in 70%–75% of human BJ fibroblasts transformed with SV40LT or HPV-E6/E7 (Figure S4B and Movie S4).

Degradation of geminin without progression through mitosis and reappearance of Cdt1 was also observed in cells that were first synchronized in G1 and then allowed to progress through endocycles in the presence of zeocin (Figure S4C and Movie S5). Immunoblotting showed that the FUCCI system faithfully reported on the rise and fall of the endogenous Cdt1 and geminin (Figures S4D and S4E) and data from FACS analysis was consistent with a prolonged G2 phase followed by entry into a 2nd S phase (Figures S4F and S4G). Furthermore, after a prolonged G2 in which APC targets were stabilized, zeocin-treated cells and POT1a/b DKO cells showed degradation of CyclinA, CyclinB, and securin (Figures S4D and S4E). In contrast, the cohesin subunit Scc1 appeared more stable. Although immunoblotting does not report on the small fraction of cohesin associated with centromeres, the persistence of Scc1 is consistent with the POT1a/b DKO diplochromosomes, which indicate retention of the centromeric cohesin.

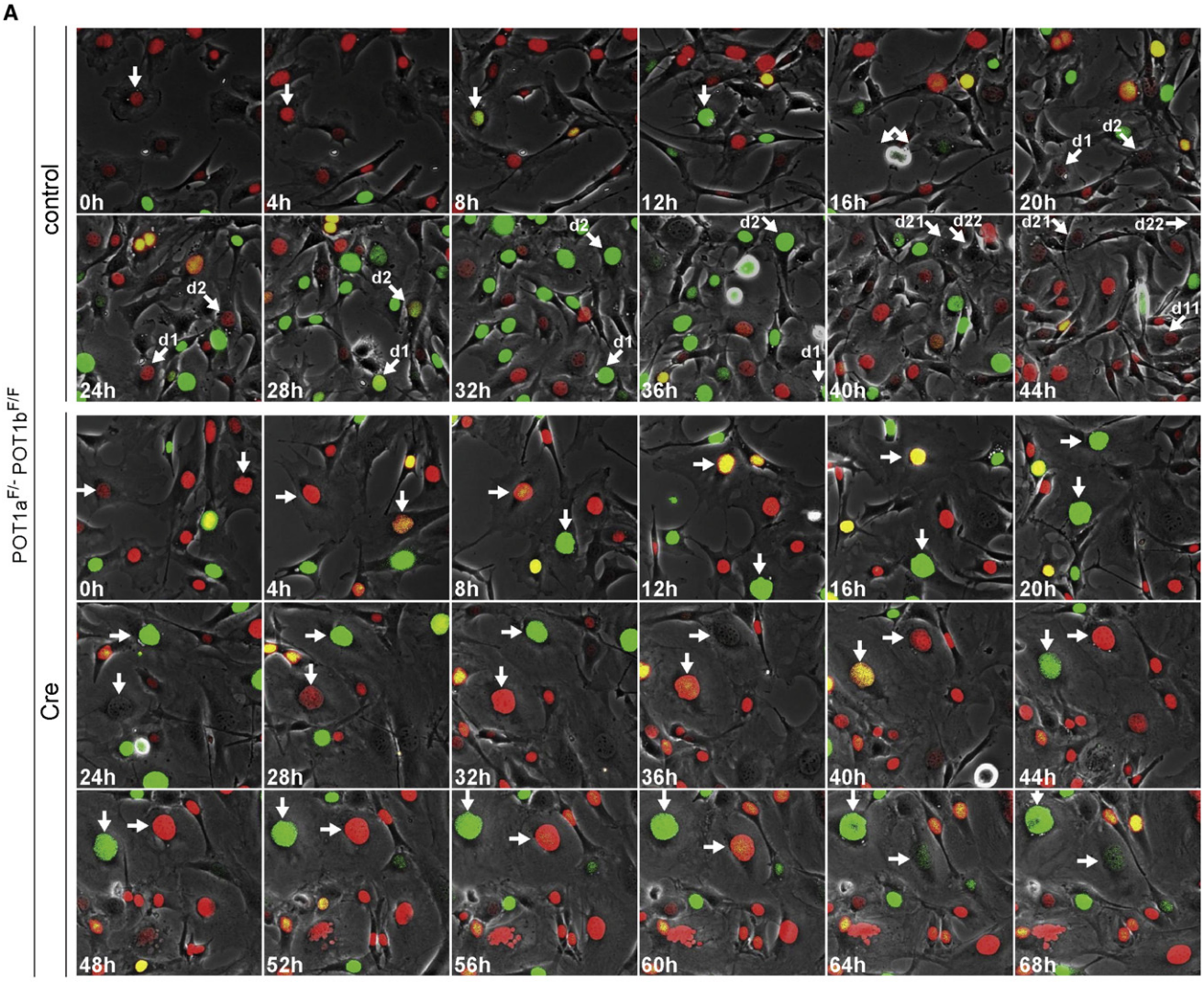

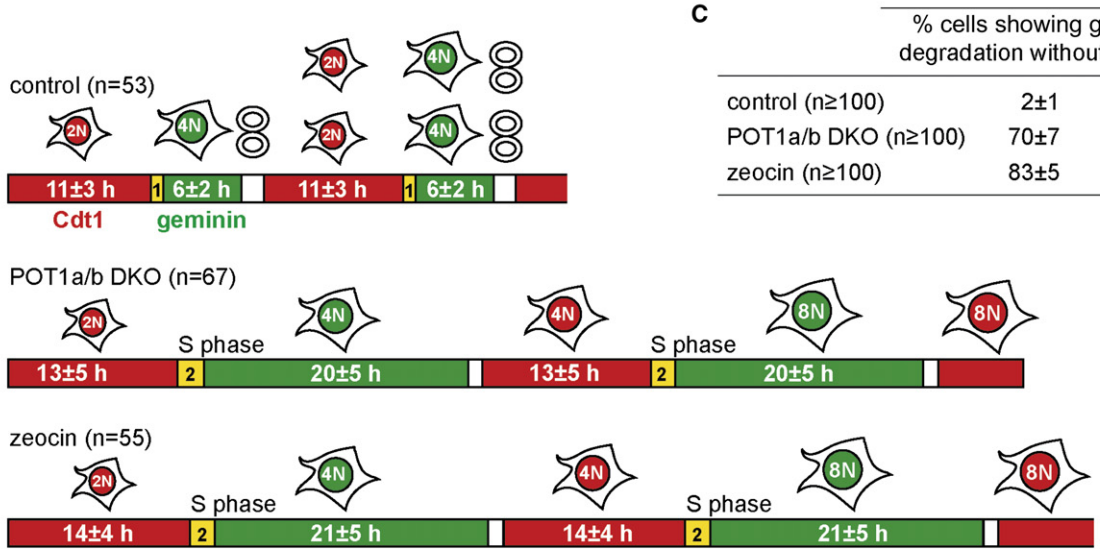

C

	% cells showing geminin degradation without mitosis
control (n≥100)	2±1
POT1a/b DKO (n≥100)	70±7
zeocin (n≥100)	83±5

Involvement of APC/Cdh1

Geminin degradation is normally mediated by APC/Cdc20 in mitosis and by APC/Cdh1 in G1. Since Cdk1/CyclinB and APC/Cdc20 appeared to be inactive in the endoreduplicating cells, we determined whether APC/Cdh1 is involved in their geminin degradation and endoreduplication. For both POT1a/b DKO cells and zeocin-treated cells, polyploidy was decreased by knockdown of Cdh1 with an shRNA (Figures 5A–5C). FUCCI imaging showed that after knockdown of Cdh1, most of POT1a/b DKO cells remained blocked in G2 (green) and geminin was not degraded in these cells whereas a parallel culture of POT1a/b DKO cells showed the mitosis-independent loss of geminin noted above (Figures 5D–5F and Movie S6). Most of the POT1a/b DKO cells treated with Cdh1 shRNA remained blocked in G2 for 30–40 hr and eventually disintegrated (Figure 5D and Movie S6). Cdh1 shRNA also had this effect on zeocin-treated cells (Figures S5A–S5C and Movie S7) and similar results were obtained with a second Cdh1 shRNA (data not shown). The occurrence of a prolonged G2 arrest is consistent with the FACS profiles in which the ratio between the 4n and 8n peaks is higher in cells treated with Cdh1 shRNA than in the control (Figure 5B). In contrast, Cdh1 knockdown in cells that were not experiencing persistent DNA damage resulted in a nearly normal progression through the cell cycle (Figures 5E and 5F and Movie S6). The role of APC/Cdh1 in the degradation of geminin and endoreduplication was further confirmed with an shRNA to the APC1 subunit of the APC, which gave similar results as the Cdh1 shRNAs (Figures S5D–S5F).

Re-establishment of Cell Division Cycles after Tetraploidization

We determined whether tetraploid cells generated by persistent telomere damage can re-enter normal cell division cycles once telomere protection is re-established. A tetracycline-inducible system was used to control POT1a expression in POT1a$^{F/-}$ POT1b$^{F/F}$ MEFs (Figure 6A). After induction of POT1a, the endogenous POT1a was removed with Cre and clonal lines were derived in which POT1a levels could be manipulated with doxycycline (Figures 6B and 6C).

This system was used to test the ability of diploid and tetraploid cells to proliferate after restoration of telomere protection. After repression of POT1a for one week, G1 diploid cells (2n) and G2 tetraploid cells (8n) were isolated by FACS-sorting (Figure 6A). Removal of doxycycline allowed re-expression of POT1a and repressed Chk1 phosphorylation (Figure 6C), indicative of the restoration of telomere protection. The cell division cycles of the resulting tetraploid and diploid populations were monitored by time-lapse imaging using H2B-GFP to visualize chromatin (Figure 6D and Movie S8). Approximately 90% of the diploid cells and ~70% of tetraploid cells were able to progress through an apparently normal cell division cycle and gave rise to viable progeny. A similar result was obtained with three out of four clones expressing inducible POT1a (data not shown). Thus, the tetraploid cells generated by persistent telomere damage can re-establish normal cell division cycles and proliferate once telomere protection is restored. As expected from their supernumary centrosomes (Figure S1B), some of the tetraploid cells showed multipolar mitotic spindles (Figure 6D), predicting a greater rate of chromosome missegregation in these clones.

DISCUSSION

These data reveal that persistent telomere damage can lead to tetraploidization and suggest a plausible scenario for the generation of aneuploid cancer cells with a subtetraploid chromosome number (Figure 7). During the early stages of tumorigenesis, before telomerase is activated, telomere shortening can eventually generate chromosome ends that no longer contain sufficient telomeric DNA for their full protection. Such cells will experience an ATM and/or ATR kinase DNA damage signal (d'Adda di Fagagna et al., 2003) resulting in permanent cell cycle arrest accompanied by senescence or apoptosis. However, in cells that escape this arrest, due to loss of the p53 pathway, persistent telomere dysfunction can induce bypass of mitosis and re-entry into S phase, resulting in tetraploid cells. Once the dysfunctional telomeres are healed by telomerase, such tetraploid clones are expected to divide and lose chromosomes at an increased rate, explaining the subtetraploid chromosome numbers observed in a large fraction of solid human cancers. Although this model emerged from the analysis of telomere damage created by shelterin deficiency, the induction of polyploidy after telomerase inhibition (Pantic et al., 2006) argues that tetraploidization can be induced by excessive telomere attrition. The model predicts that tetraploidization takes place early in tumorigenesis during the period of telomere dysfunction before telomerase is activated. Furthermore, it predicts that telomere-driven tetraploidization occurs in the subset of human cancers that show loss of p53 function as an early step.

The Mechanism of Telomere-Driven Tetraploidization

Our data illuminate the mechanism by which telomere dysfunction induces the formation of tetraploid cells in absence of p53.

Figure 4. Geminin and Cdt1 Alternate in POT1a/b DKO and Zeocin-Treated Cells

(A) FUCCI imaging of geminin and Cdt1. Time lapse imaging of POT1a$^{F/-}$POT1b$^{F/F}$ MEFs transduced with FUCCI lentiviral vectors, expressing mKO2-hCdt1 (red) and mAG-hGeminin (green). Cells were treated with Cre or vector control and imaged after 72 hr. Phase-contrast images and fluorescent images using GFP and rhodamine filters were taken every 15 min (Movie S3). Selected time points are shown. Arrows with the same orientation highlight the same cell at different times. In control cells, arrows highlight one cell progressing through a normal cell cycle (red-yellow-green, mitosis) and its daughters until they move out of the field. In Cre-treated cells, arrows highlight two representative cells showing the color sequence red-yellow-green-red-yellow-green without intervening mitotis.

(B) Duration of alternating geminin and Cdt1 expression in endoreduplicating cells. POT1a$^{F/-}$POT1b$^{F/F}$ MEFs treated with vector control, Cre, (POT1a/b DKO) or zeocin (Movie S3) were imaged as in (A). The indicated number of cells was followed throughout the imaging session and the length of G1 (red), entry into S phase (yellow) and S/G2 (green) was measured. Average values (hr) are shown. See also related Figure S4A.

(C) Quantification of geminin degradation in the absence of mitosis. Cells were treated and imaged as above and the movies were analyzed for cells showing at least one event of geminin degradation in the absence of mitosis. > 100 cells were scored for each condition. Average values and SDs were obtained from four independent experiments. See also related Figure S4.

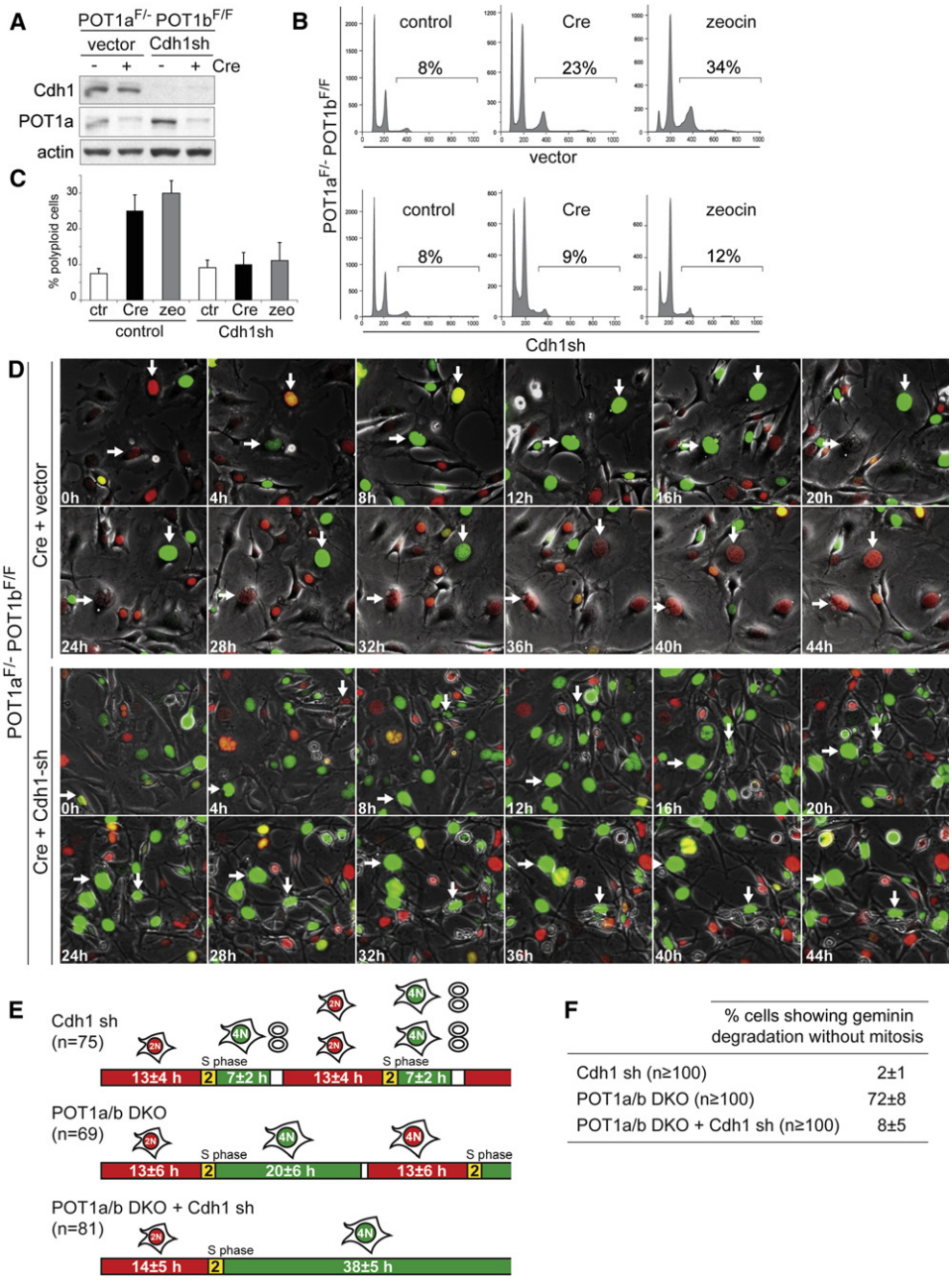

Figure 5. Involvement of Cdh1 in Endoreduplication

(A–C) Knockdown of Cdh1 inhibits polyploidization. POT1a$^{F/-}$POT1b$^{F/F}$ MEFs were treated with shRNA to knockdown Cdh1 (immunoblot in [A]), and polyploidy was measured after POT1a/b deletion by Cre expression, zeocin treatment, or in untreated cells. FACS profiles from a representative experiment (B) and quantification of the percentage of polyploid cells in three independent experiments with SDs (C) are shown.

(D) Diminished geminin degradation after Cdh1 knockdown. POT1a$^{F/-}$POT1b$^{F/F}$ MEFs transduced with FUCCI vectors were treated with Cre, followed by Cdh1 shRNA or vector control infections a day later. Two days later, the cells were imaged for 60 hr (Movie S6) and selected time points of a representative experiment are shown. Arrows with the same orientation highlight the same cell over time. In Cre-treated cells two representative cells showing geminin degradation without mitosis are highlighted. In cells treated with Cre and Cdh1 shRNA, arrows highlight two cells showing prolonged arrest in G2 and persistence of geminin.

(E) Schematic of FUCCI imaging data obtained on POT1a/b DKO cells treated with Cdh1 shRNA. Cells were treated and imaged as in (D). Cells treated with Cdh1 shRNA only were imaged separately (Movie S6). The indicated number of cells were followed throughout the imaging session to determine the length of G1 (red), entry into S phase (yellow), and S/G2 (green). Average values (hr) are shown.

(F) Table showing the effect of Cdh1 knockdown on mitosis-independent geminin degradation. Cells were treated and imaged as in (D) and (E). At least 100 cells were followed throughout the movie and the percentage of cells showing at least one event of geminin degradation without mitosis was determined. Average values and SDs were obtained from three independent experiments.

See also related Figure S5.

The endoreduplication event occurs in response to a persistent DNA damage signal elicited by telomeres that are permanently damaged. The resulting ATM/ATR and Chk1/Chk2 signaling cascade prevents activation of Cdk1/CyclinB, thereby blocking entry into mitosis and extending G2. Despite the lack of progression through mitosis, the cells eventually switch to a state resembling G1. Importantly, the DNA replication inhibitor geminin, which prevents rereplication in G2, is degraded whereas Cdt1, which is required for origin licensing, is re-expressed. As a result of this altered state, cells re-enter S phase and become tetraploid.

Our findings are consistent with work in fission yeast and human cells showing rereplication upon inhibition of the mitotic Cdk/cyclin (Hayles et al., 1994; Kiang et al., 2009; Itzhaki et al., 1997) and with early observations on the uncoupling of S and M phase in IR-treated p21-deficient cells (Waldman et al., 1996; Lanni and Jacks, 1998). The dependence of origin relicensing on low Cdk activity explains how persistent Cdk inactivation permits rereplication (Diffley, 2004). We also find that Cdh1 is important for endoreduplication, most likely because it mediates the degradation of geminin. In agreement, Cdh1 is required for endocycles in placental trophoblasts and in the *Drosophila* salivary gland (Garcia-Higuera et al., 2008; Narbonne-Reveau et al., 2008; Zielke et al., 2008; Li et al., 2008). Previous work indicates that APC/Cdh1 can be activated by the DNA damage response through a mechanism involving Cdc14B phosphatase (Bassermann et al., 2008). In the context of telomere damage, however, the degradation of geminin may simply be due to a gradual rise in APC/Cdh1 activity during the prolonged postreplication period without Cdk1/CyclinB, which would normally inhibit APC/Cdh1 until mitosis is completed.

Our data also shed light on previous reports of endoreduplication and diplochromosomes in human and mouse cells after inhibition of Nbs1, Rad17, and XRCC3 (Reina-San-Martin et al., 2005; Wang et al., 2003; Yoshihara et al., 2004). As it is likely that these cells experience a persistent DNA damage signal, we propose that the endoreduplication observed in these settings involves the pathway described here.

The Causes of Tetraploidization in Cancer

Tetraploidy can be experimentally induced in p53 null cells by transient inhibition of the actin cytoskeleton or by virus-mediated cell fusion and has been shown to promote tumorigenic transformation (Fujiwara et al., 2005; Duelli et al., 2007). Tetraploidization has also been suggested to be one of the outcomes of chromosome nondisjunction (Shi and King, 2005), possibly through a lagging chromosome blocking the cleavage furrow (but see Weaver et al., 2006). Arguably more directly relevant to human tumorigenesis are the findings that polyploidy can be induced by loss of the tumor suppressor APC (adenomatosis polyposis coli) (Caldwell et al., 2007) or overexpression of the E2F target Mad2 (Sotillo et al., 2007; Dikovskaya et al., 2007).

Telomere-driven tetraploidization adds to these pathways and is noteworthy, because it is a natural consequence of overproliferation of premalignant cells. Unlike the other potential causes of tetraploidization, the telomere-dependent pathway does not require genetic alterations other than the loss of p53, which is a general requirement for the survival of tetraploid cells. Telomere-driven tetraploidization relies on replicative telomere shortening—a pathway that is operational in the early stages of a wide range of human cancers. Importantly, the DNA damage signal that induces tetraploidization is a temporary phenomenon, as the DNA damage signal is expected to dissipate when telomerase is activated or telomere function is restored in another way. Our data indicate that once telomere protection is re-established, tetraploid cells can proliferate through apparently normal cell division cycles.

Telomere Damage in p53-Deficient Cells: A Perfect Storm

Previous work has shown that diminished telomere function results in end-to-end fusion of chromosomes (van Steensel et al., 1998; Lee et al., 1998). In p53-deficient cells, the resulting dicentric chromosomes can initiate breakage-fusion-bridge cycles that promote the main genomic alterations observed in cancer: loss of heterozygosity, gene amplification, and nonreciprocal translocations (Artandi et al., 2000; Maser and DePinho, 2002). The telomere-driven tetraploidization described here is likely to provide a considerable advantage to cells experiencing this type of genome instability, since it diminishes the chance that an essential gene is lost. Telomere dysfunction could create a perfect storm in the genome—a combination of tetraploidization and genome rearrangements—resulting in progeny with extensively altered subtetraploid genomes on which selection for the most malignant clone can take place. Cells surviving this crisis will likely have activated telomerase, which can restore telomere function and thus dampen the ongoing genome instability.

The proposal that telomere-driven genome instability is a major contributing factor in human cancer is not at variance with the view that telomere attrition represents a tumor suppressor mechanism. Previous work has highlighted the differential effect of telomere attrition depending on the p53 status of the cells (Chin et al., 1999; Artandi et al., 2000; de Lange and Jacks, 1999). When the p53 pathway is intact, telomere attrition can limit proliferation and thereby suppress tumorigenesis. The effects described here only take place once this key tumor suppressor pathway has failed.

EXPERIMENTAL PROCEDURES

Isolation of MEFs, Cell Culture Procedures, and Viral Gene Delivery

POT1a/b DKO MEFs lacking ATM were generated by intercrosses of POT1a$^{F/-}$ POT1b$^{F/F}$ (Hockemeyer et al., 2006) and ATM$^{+/-}$ (Barlow et al., 1996) mice. MEFs were isolated, SV40LT-immortalized, and treated with retroviral Cre as described (Hockemeyer et al., 2006). Human BJ fibroblasts (p40) expressing HPV-E6/E7 or SV40LT were maintained in DMEM/10% FBS. Lentiviral vectors (pLK0.1) containing shRNA for Chk1 (#RMM3981-9580337 [set1] and RMM3981-9580340 [set2]), Chk2 (RMM3981-9580345 [set1] and RMM3981-9580346 [set2]), Cdh1 (RMM3981-9593724), and ANAPC1 (RMM3981-97076474) were from Open Biosystem. The ATR shRNA retroviral vector was as described (Denchi and de Lange, 2007). Infections with sRNAs were performed one day after infection with Cre. For CyclinE-eGFP, the C terminus of full-length hCyclinE (provided by J. Pines) was fused to eGFP in pLPC. FUCCI lentiviral vectors were provided by A. Miyawaki (Sakaue-Sawano et al., 2008). Viral transduction was performed using 2–4 infections of 4–6 hr each. TopBP1-ER was provided by O. Fernandez-Capetillo (Toledo et al., 2008). Zeocin (Invitrogen, 100 μg/ml), doxorubicin (Sigma, 1 μM), and bleomycin (Sigma, 50 μg/ml) were added to culture media every 2 or 3 days. Cells

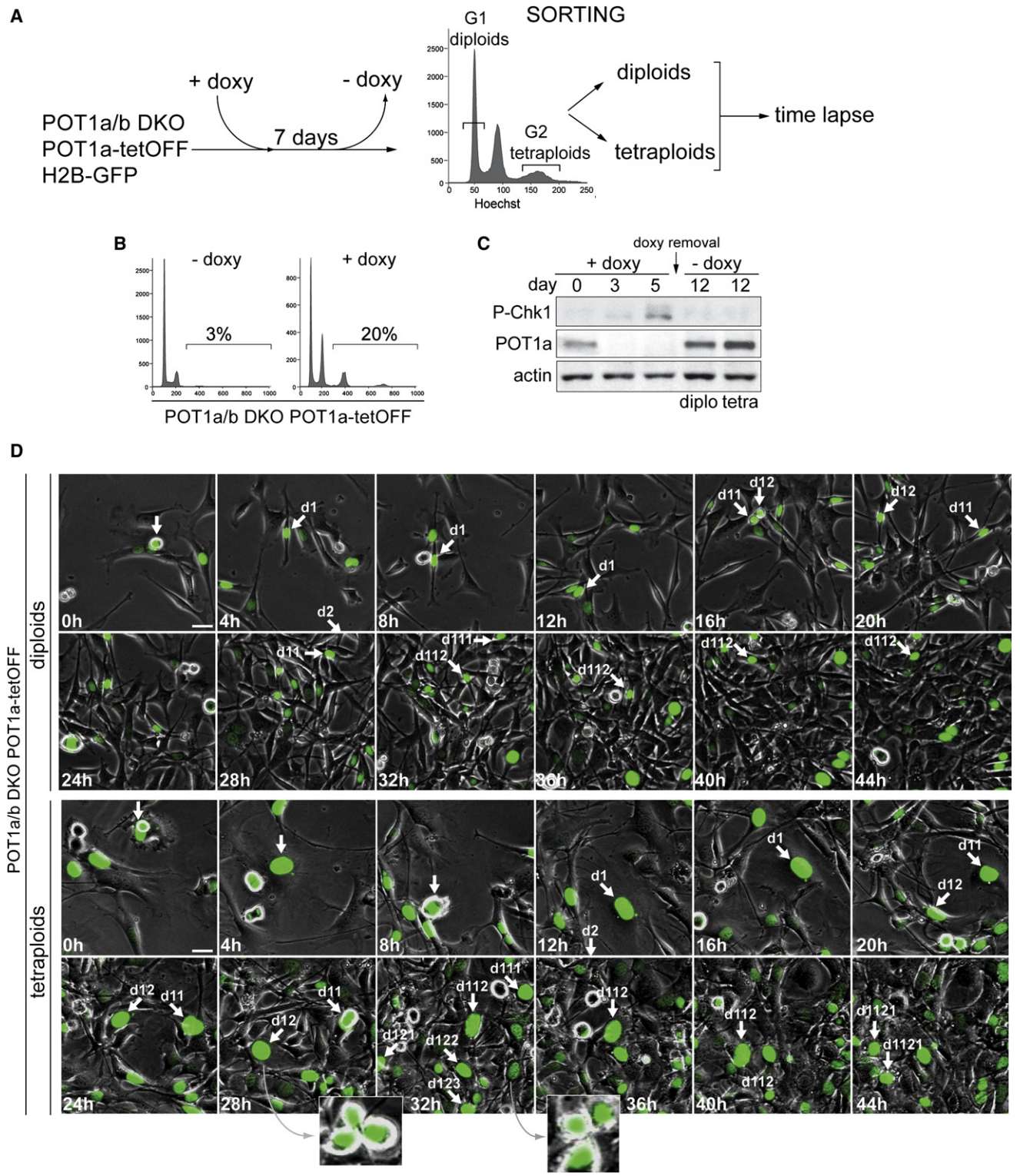

Figure 6. Re-establishment of Cell Division Cycles after Tetraploidization

(A) Schematics of the experimental approach. H2B-GFP expressing cells POT1a$^{F/-}$POT1b$^{F/F}$ MEFs transduced with POT1a under the control of the Tet-Off inducible promoter were treated with Cre and cloned. Data on one clone (#19) is shown. After 7 days of treatment with doxycycline (doxy) to repress POT1a, cell line #19 was stained with Hoechst and FACS-sorted for DNA content. G1 diploid cells (2n peak) and G2 tetraploid cells (8n peak) were separated, plated in the absence of doxyxycline and monitored by time lapse imaging.

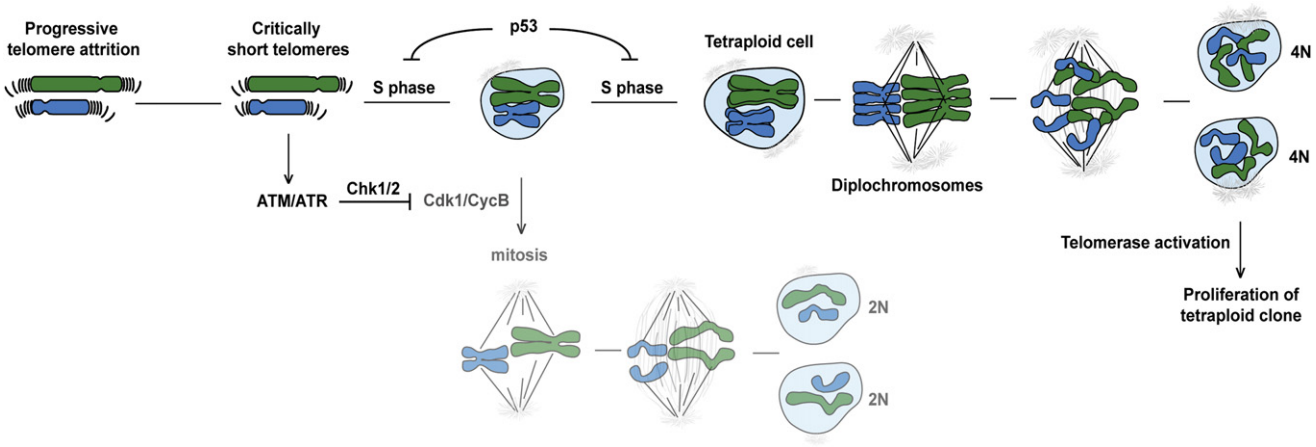

Figure 7. Model for Telomere-Driven Tetraploidization in Cancer

Simplified cartoon illustrating how telomere attrition might induce tetraploidization. Critically short telomeres resulting from telomere attrition are proposed to lead to a persistent DNA damage response. In p53-deficient cells, no G1/S arrest and senescence/apoptotic response to the DNA damage will occur. Activation of the ATM/ATR kinase pathway will lead to permanent inhibition of Cdk1/CyclinB, blocking mitosis. The cells are then able to bypass mitosis and re-enter S phase (due to the degradation of geminin by APC/Cdh1), becoming tetraploid. Some of these cells might carry diplochromosomes as shown in the cartoon. Activation or upregulation of telomerase will be required for the restoration of telomere function, thereby silencing the DNA damage response and allowing proliferation of tetraploid clones.

were blocked in G1/S by using two o/n treatments with 2 mM thymidine separated by 10 hr incubation in regular media.

FACS

FACS analysis for DNA content was performed using standard procedures and PI DNA staining. For BrdU staining, cells were pulsed with 10 μM BrdU (Sigma) for 60 min, fixed, and incubated with FITC-conjugated anti-BrdU antibody (BD Biosciences). Flow cytometry was performed using the FACS calibur (Becton Dickinson) and data were analyzed using FlowJo 8.7.1 software. To calculate the percentage of polyploid cells (DNA content > 4n), cell doublets and sub-G1 apoptotic cells were excluded. Diploid and tetraploid cells were isolated by sorting for a G1 diploid DNA content or a G2 tetraploid DNA content using an BD FACSAria-2 cell sorter (BD Biosciences) after incubation with Hoechst 33342 (10 μM, AnaSpec, Inc.) for 30 min.

IF and Immunoblotting

IF and immunoblotting were performed using standard procedures described previously (Celli and de Lange, 2005) using the following antibodies: POT1a (1221) and POT1b (1223) (Hockemeyer et al., 2006); ATR N-19 (sc-1887, Santa Cruz); Chk1 (sc-8408, Santa Cruz); Chk1 pS345 (#2348, Cell Signaling Technology); Chk2 (611570, BD Biosciences); CyclinE M-20 (sc-481, Santa Cruz); CyclinA (sc-596, Santa Cruz), CyclinB1 (sc-245, Santa Cruz); AuroraA (ab13824, Abcam); AuroraB (ab2254, Abcam); Plk1 (#06-813, Upstate); securin (K0090-3, MBL); Cdc20 (ab64877, Abcam); Cdh1 (ab5483, Abcam); geminin (sc-13015, Santa Cruz); β-actin (I-19) (sc-1616, Santa Cruz); Cdk1 (cc16, Calbiochem); Cdk2 (M2) (sc-163, Santa Cruz); APC1 (NB 100-86985, Novus Biologicals); Cdt1 (P26A6, a gift from A. Ballabeni [Ballabeni et al., 2004]); Cdk1 P-Tyr14/15 (#9111, Cell Signaling); pericentrin (ab4448 Abcam); Scc1 (K0202-3, MBL). IF for 53BP1 was performed with Ab 100-304A (Novus Biologicals).

Cdk Kinase Assay

Cells ($1 \cdot 10^6$ cells plated the day before) were washed once with ice-cold PBS, resuspended in lysis buffer (0.3% Triton X-100, 50 mM sodium phosphate [pH 7.2], 2 mM EDTA, 2 mM EGTA, 25 mM NaF, 100 μM $NaVO_4$, 25 mM 2-glycerophosphate, 1 mM PMSF, and a protease inhibitor cocktail (Roche Diagnostics)) and frozen in liquid nitrogen. Thawed extracts were sonicated, cleared after incubation with Protein G Sepharose (GE Healthcare), and incubated with anti-CyclinB1 (sc-245, Santa Cruz), anti-CyclinE M-20 (sc-481, Santa Cruz), or control IgG for 2 hr. After 45 min with Protein G Sepharose beads, IPs were collected and washed three times in lysis buffer. Kinase activities were determined by incubating beads with H1 (5 μg, Roche) in kinase reaction buffer (50 mM HEPES [pH 7.5], 10 mM $MgCl_2$, 50 mM 2-glycerophosphate, 0.1% Triton X-100, 1 mM DTT) with 150 μl/ml ^{32}P-γ-ATP (10 μCi/μl) for 10 min at 30°C. Laemmli buffer was added and samples were fractionated on SDS-PAGE. H1-P was detected using a Storm PhosphorImager (Amersham). Kinase activity was quantified using ImageQuant software and normalized to the amounts of H1 and Cdk1 or Cdk2 in the IPs (ImageJ software).

Live-Cell Imaging

Live-cell imaging was started at day 3 after Cre and/or 2 days after treatment with Cdh1 shRNA; zeocin was added 2 hr before the imaging session and maintained in the culture medium. Cells were grown on a 4-chambered coverglass (Lab-Tek) in phenol red-free Liebovitz's L-15 medium (GIBCO) containing 15% FBS. Time-lapse live-cell imaging was performed using an Olympus IX71 inverted microscope (Olympus America, Inc.) and MetaMorph software (Universal Imaging, Media, PA). Phase-contrast and fluorescent (GFP and RFP filters) images were acquired every 15 min with a 10× objective. For CyclinE-eGFP expressing cells, a 20× objective was used. Image analysis was performed using MetaMorph or ImageJ software. Nuclear size was calculated from digital images using the Openlab (Improvision) measure module and statistical analysis was performed using a nonparametric Krustal-Wallis test (Prism software).

(B) Induction of polyploidy after treatment with doxycycline. Clone #19 described in (A) was analyzed by FACS (PI staining) after 7 days in doxycycline.
(C) Reversible expression of POT1a and silencing of the DNA damage signal. Immunoblotting for the indicated proteins in cell line #19 is shown after 3 or 5 days of doxycycline treatment and 5 days after its removal (day 12) in sorted diploid and tetraploid cells.
(D) Cell divisions of diploid and tetraploid cells derived from clone #19 after re-expression of POT1a. Time lapse imaging of diploid and tetraploid cells expressing H2B-GFP was started 24 hr after doxyxcycline removal. Phase-contrast and GFP-fluorescent images were taken every 15 min (Movie S8). Selected time points are shown. Arrows highlight a cell performing multiple cell divisions during the imaging session. Insets show evidence for multipolar mitoses.

Tet-Off Inducible System for POT1a Expression

POT1a cloned into P-TRE-Tight (Clonetech) and P-Tet-Off-Advanced (Clonetech) were transduced into H2B-GFP expressing POT1a$^{F/-}$POT1b$^{F/F}$ MEFs. After treatment with Cre, clones were isolated with cloning cylinders and analyzed by PCR for the deletion of the endogenous POT1a. Clones were tested for doxycyclin (1 μg/ml) controlled expression of POT1a and polyploidization. Four clones were selected for further analysis; data on one clone (#19) is presented.

SUPPLEMENTAL INFORMATION

Supplemental Information includes five figures and eight movies and can be found with this article online at doi:10.1016/j.cell.2010.01.031.

ACKNOWLEDGMENTS

We thank Devon White for expert mouse husbandry. Antibodies, DNA constructs, and protocols were generously provided by Drs. A. Ballabeni, J. Pines, A. Miyawaki, and O. Fernandez-Capetillo. We are grateful to Dr. A. Musacchio, Dr. D. Morgan, and members of the de Lange lab for advice and discussion. A. North (RU Bio-imaging RC) and S. Mazel (RU Flow Cytometry RC) are thanked for expert assistance. This work was supported by the Breast Cancer Research Foundation.

Received: September 22, 2009
Revised: December 9, 2009
Accepted: January 15, 2010
Published: April 1, 2010

REFERENCES

Andreassen, P.R., Lohez, O.D., Lacroix, F.B., and Margolis, R.L. (2001). Tetraploid state induces p53-dependent arrest of nontransformed mammalian cells in G1. Mol. Biol. Cell *12*, 1315–1328.

Artandi, S.E., Chang, S., Lee, S.L., Alson, S., Gottlieb, G.J., Chin, L., and DePinho, R.A. (2000). Telomere dysfunction promotes non-reciprocal translocations and epithelial cancers in mice. Nature *406*, 641–645.

Ballabeni, A., Melixetian, M., Zamponi, R., Masiero, L., Marinoni, F., and Helin, K. (2004). Human geminin promotes pre-RC formation and DNA replication by stabilizing CDT1 in mitosis. EMBO J. *23*, 3122–3132.

Barlow, C., Hirotsune, S., Paylor, R., Liyanage, M., Eckhaus, M., Collins, F., Shiloh, Y., Crawley, J.N., Ried, T., Tagle, D., and Wynshaw-Boris, A. (1996). Atm-deficient mice: a paradigm of ataxia telangiectasia. Cell *86*, 159–171.

Bassermann, F., Frescas, D., Guardavaccaro, D., Busino, L., Peschiaroli, A., and Pagano, M. (2008). The Cdc14B-Cdh1-Plk1 axis controls the G2 DNA-damage-response checkpoint. Cell *134*, 256–267.

Blow, J.J., and Dutta, A. (2005). Preventing re-replication of chromosomal DNA. Nat. Rev. Mol. Cell Biol. *6*, 476–486.

Bodnar, A.G., Ouellette, M., Frolkis, M., Holt, S.E., Chiu, C.P., Morin, G.B., Harley, C.B., Shay, J.W., Lichtsteiner, S., and Wright, W.E. (1998). Extension of life-span by introduction of telomerase into normal human cells. Science *279*, 349–352.

Caldwell, C.M., Green, R.A., and Kaplan, K.B. (2007). APC mutations lead to cytokinetic failures in vitro and tetraploid genotypes in Min mice. J. Cell Biol. *178*, 1109–1120.

Carder, P., Wyllie, A.H., Purdie, C.A., Morris, R.G., White, S., Piris, J., and Bird, C.C. (1993). Stabilised p53 facilitates aneuploid clonal divergence in colorectal cancer. Oncogene *8*, 1397–1401.

Celli, G.B., and de Lange, T. (2005). DNA processing not required for ATM-mediated telomere damage response after TRF2 deletion. Nat. Cell Biol. *7*, 712–718.

Chin, K., De Solorzano, C.O., Knowles, D., Jones, A., Chou, W., Rodriguez, E.G., Kuo, W.L., Ljung, B.M., Chew, K., Myambo, K., et al. (2004). In situ analyses of genome instability in breast cancer. Nat. Genet. *36*, 984–988.

Chin, L., Artandi, S.E., Shen, Q., Tam, A., Lee, S.L., Gottlieb, G.J., Greider, C.W., and DePinho, R.A. (1999). p53 deficiency rescues the adverse effects of telomere loss and cooperates with telomere dysfunction to accelerate carcinogenesis. Cell *97*, 527–538.

d'Adda di Fagagna, F., Reaper, P.M., Clay-Farrace, L., Fiegler, H., Carr, P., Von Zglinicki, T., Saretzki, G., Carter, N.P., and Jackson, S.P. (2003). A DNA damage checkpoint response in telomere-initiated senescence. Nature *426*, 194–198.

Danes, B.S. (1978). Increased in vitro tetraploidy: tissue specific within the heritable colorectal cancer syndromes with polyposis coli. Cancer *41*, 2330–2334.

de Lange, T., and Jacks, T. (1999). For better or worse? Telomerase inhibition and cancer. Cell *98*, 273–275.

de Lange, T., Shiue, L., Myers, R.M., Cox, D.R., Naylor, S.L., Killery, A.M., and Varmus, H.E. (1990). Structure and variability of human chromosome ends. Mol. Cell. Biol. *10*, 518–527.

Denchi, E.L., and de Lange, T. (2007). Protection of telomeres through independent control of ATM and ATR by TRF2 and POT1. Nature *448*, 1068–1071.

Diffley, J.F. (2004). Regulation of early events in chromosome replication. Curr. Biol. *14*, R778–R786.

Dikovskaya, D., Schiffmann, D., Newton, I.P., Oakley, A., Kroboth, K., Sansom, O., Jamieson, T.J., Meniel, V., Clarke, A., and Nathke, I.S. (2007). Loss of APC induces polyploidy as a result of a combination of defects in mitosis and apoptosis. J. Cell Biol. *176*, 183–195.

Duelli, D.M., Padilla-Nash, H.M., Berman, D., Murphy, K.M., Ried, T., and Lazebnik, Y. (2007). A virus causes cancer by inducing massive chromosomal instability through cell fusion. Curr. Biol. *17*, 431–437.

Dutrillaux, B., Gerbault-Seureau, M., Remvikos, Y., Zafrani, B., and Prieur, M. (1991). Breast cancer genetic evolution: I. Data from cytogenetics and DNA content. Breast Cancer Res. Treat. *19*, 245–255.

Fujiwara, T., Bandi, M., Nitta, M., Ivanova, E.V., Bronson, R.T., and Pellman, D. (2005). Cytokinesis failure generating tetraploids promotes tumorigenesis in p53-null cells. Nature *437*, 1043–1047.

Galipeau, P.C., Cowan, D.S., Sanchez, C.A., Barrett, M.T., Emond, M.J., Levine, D.S., Rabinovitch, P.S., and Reid, B.J. (1996). 17p (p53) allelic losses, 4N (G2/tetraploid) populations, and progression to aneuploidy in Barrett's esophagus. Proc. Natl. Acad. Sci. USA *93*, 7081–7084.

Ganem, N.J., Storchova, Z., and Pellman, D. (2007). Tetraploidy, aneuploidy and cancer. Curr. Opin. Genet. Dev. *17*, 157–162.

Garcia-Higuera, I., Manchado, E., Dubus, P., Canamero, M., Mendez, J., Moreno, S., and Malumbres, M. (2008). Genomic stability and tumour suppression by the APC/C cofactor Cdh1. Nat. Cell Biol. *10*, 802–811.

Hastie, N.D., Dempster, M., Dunlop, M.G., Thompson, A.M., Green, D.K., and Allshire, R.C. (1990). Telomere reduction in human colorectal carcinoma and with ageing. Nature *346*, 866–868.

Hayles, J., Fisher, D., Woollard, A., and Nurse, P. (1994). Temporal order of S phase and mitosis in fission yeast is determined by the state of the p34cdc2-mitotic B cyclin complex. Cell *78*, 813–822.

Hockemeyer, D., Daniels, J.P., Takai, H., and de Lange, T. (2006). Recent expansion of the telomeric complex in rodents: Two distinct POT1 proteins protect mouse telomeres. Cell *126*, 63–77.

Itzhaki, J.E., Gilbert, C.S., and Porter, A.C. (1997). Construction by gene targeting in human cells of a "conditional" CDC2 mutant that rereplicates its DNA. Nat. Genet. *15*, 258–265.

Kiang, L., Heichinger, C., Watt, S., Bahler, J., and Nurse, P. (2009). Cyclin-dependent kinase inhibits reinitiation of a normal S-phase program during G2 in fission yeast. Mol. Cell. Biol. *29*, 4025–4032.

Kim, N.W., Piatyszek, M.A., Prowse, K.R., Harley, C.B., West, M.D., Ho, P.L., Coviello, G.M., Wright, W.E., Weinrich, S.L., and Shay, J.W. (1994). Specific association of human telomerase activity with immortal cells and cancer. Science *266*, 2011–2015.

Kops, G.J., Weaver, B.A., and Cleveland, D.W. (2005). On the road to cancer: aneuploidy and the mitotic checkpoint. Nat. Rev. Cancer *5*, 773–785.

Lanni, J.S., and Jacks, T. (1998). Characterization of the p53-dependent postmitotic checkpoint following spindle disruption. Mol. Cell. Biol. *18*, 1055–1064.

Lee, H.W., Blasco, M.A., Gottlieb, G.J., Horner, J.W., 2nd, Greider, C.W., and DePinho, R.A. (1998). Essential role of mouse telomerase in highly proliferative organs. Nature *392*, 569–574.

Levine, D.S., Rabinovitch, P.S., Haggitt, R.C., Blount, P.L., Dean, P.J., Rubin, C.E., and Reid, B.J. (1991). Distribution of aneuploid cell populations in ulcerative colitis with dysplasia or cancer. Gastroenterology *101*, 1198–1210.

Li, M., Shin, Y.H., Hou, L., Huang, X., Wei, Z., Klann, E., and Zhang, P. (2008). The adaptor protein of the anaphase promoting complex Cdh1 is essential in maintaining replicative lifespan and in learning and memory. Nat. Cell Biol. *10*, 1083–1089.

Maser, R.S., and DePinho, R.A. (2002). Connecting chromosomes, crisis, and cancer. Science *297*, 565–569.

Narbonne-Reveau, K., Senger, S., Pal, M., Herr, A., Richardson, H.E., Asano, M., Deak, P., and Lilly, M.A. (2008). APC/CFzr/Cdh1 promotes cell cycle progression during the Drosophila endocycle. Development *135*, 1451–1461.

Olaharski, A.J., Sotelo, R., Solorza-Luna, G., Gonsebatt, M.E., Guzman, P., Mohar, A., and Eastmond, D.A. (2006). Tetraploidy and chromosomal instability are early events during cervical carcinogenesis. Carcinogenesis *27*, 337–343.

Pantic, M., Zimmermann, S., El Daly, H., Opitz, O.G., Popp, S., Boukamp, P., and Martens, U.M. (2006). Telomere dysfunction and loss of p53 cooperate in defective mitotic segregation of chromosomes in cancer cells. Oncogene *25*, 4413–4420.

Peters, J.M. (2002). The anaphase-promoting complex: proteolysis in mitosis and beyond. Mol. Cell *9*, 931–943.

Rabinovitch, P.S., Reid, B.J., Haggitt, R.C., Norwood, T.H., and Rubin, C.E. (1989). Progression to cancer in Barrett's esophagus is associated with genomic instability. Lab. Invest. *60*, 65–71.

Reina-San-Martin, B., Nussenzweig, M.C., Nussenzweig, A., and Difilippantonio, S. (2005). Genomic instability, endoreduplication, and diminished Ig class-switch recombination in B cells lacking Nbs1. Proc. Natl. Acad. Sci. USA *102*, 1590–1595.

Sakaue-Sawano, A., Kurokawa, H., Morimura, T., Hanyu, A., Hama, H., Osawa, H., Kashiwagi, S., Fukami, K., Miyata, T., Miyoshi, H., et al. (2008). Visualizing spatiotemporal dynamics of multicellular cell-cycle progression. Cell *132*, 487–498.

Shi, Q., and King, R.W. (2005). Chromosome nondisjunction yields tetraploid rather than aneuploid cells in human cell lines. Nature *437*, 1038–1042.

Sotillo, R., Hernando, E., Diaz-Rodriguez, E., Teruya-Feldstein, J., Cordon-Cardo, C., Lowe, S.W., and Benezra, R. (2007). Mad2 overexpression promotes aneuploidy and tumorigenesis in mice. Cancer Cell *11*, 9–23.

Storchova, Z., and Kuffer, C. (2008). The consequences of tetraploidy and aneuploidy. J. Cell Sci. *121*, 3859–3866.

Toledo, L.I., Murga, M., Gutierrez-Martinez, P., Soria, R., and Fernandez-Capetillo, O. (2008). ATR signaling can drive cells into senescence in the absence of DNA breaks. Genes Dev. *22*, 297–302.

van Steensel, B., Smogorzewska, A., and de Lange, T. (1998). TRF2 protects human telomeres from end-to-end fusions. Cell *92*, 401–413.

Waldman, T., Lengauer, C., Kinzler, K.W., and Vogelstein, B. (1996). Uncoupling of S phase and mitosis induced by anticancer agents in cells lacking p21. Nature *381*, 713–716.

Wang, X., Zou, L., Zheng, H., Wei, Q., Elledge, S.J., and Li, L. (2003). Genomic instability and endoreduplication triggered by RAD17 deletion. Genes Dev. *17*, 965–970.

Weaver, B.A., Silk, A.D., and Cleveland, D.W. (2006). Cell biology: nondisjunction, aneuploidy and tetraploidy. Nature *442*, E9–E10.

Yoshihara, T., Ishida, M., Kinomura, A., Katsura, M., Tsuruga, T., Tashiro, S., Asahara, T., and Miyagawa, K. (2004). XRCC3 deficiency results in a defect in recombination and increased endoreduplication in human cells. EMBO J. *23*, 670–680.

Zielke, N., Querings, S., Rottig, C., Lehner, C., and Sprenger, F. (2008). The anaphase-promoting complex/cyclosome (APC/C) is required for rereplication control in endoreplication cycles. Genes Dev. *22*, 1690–1703.

Cell

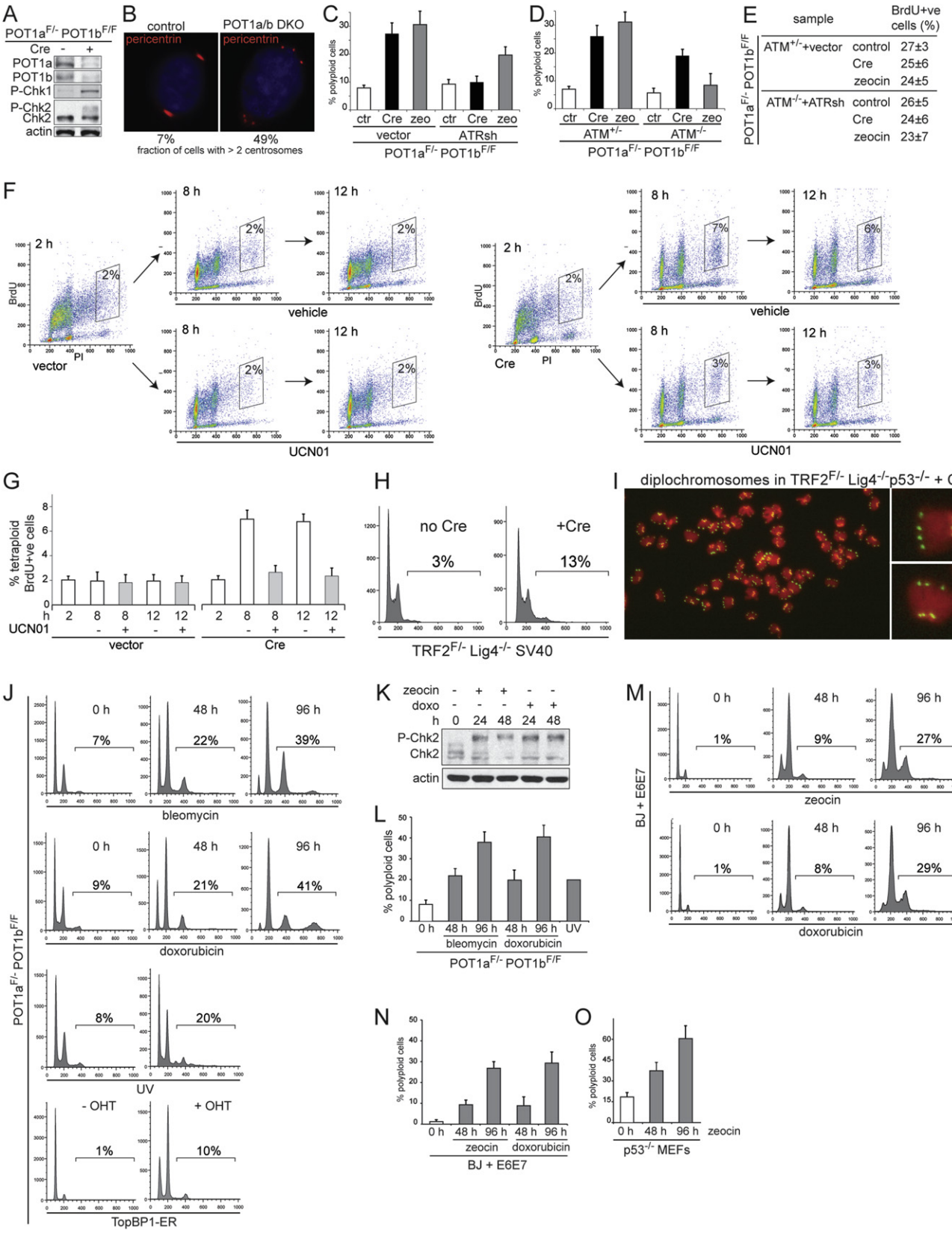
A
POT1a F/- POT1b F/F
Cre - +
POT1a
POT1b
P-Chk1
P-Chk2
Chk2
actin
B
control
POT1a/b DKO
pericentrin
pericentrin
7%
49%
fraction of cells with > 2 centrosomes
C
% polyploid cells
ctr Cre zeo ctr Cre zeo
vector ATRsh
POT1a F/- POT1b F/F
D
% polyploid cells
ctr Cre zeo ctr Cre zeo
ATM +/- ATM -/-
POT1a F/- POT1b F/F
E
POT1a F/- POT1b F/F
sample
BrdU+ve cells (%)
ATM +/-+vector control 27±3
Cre 25±6
zeocin 24±5
ATM -/-+ATRsh control 26±5
Cre 24±6
zeocin 23±7
F
2 h
8 h
12 h
BrdU
PI
vector
vehicle
UCN01
Cre
G
% tetraploid BrdU+ve cells
h 2 8 8 12 12 2 8 8 12 12
UCN01 - + - + - + - + - +
vector
Cre
H
no Cre
3%
+Cre
13%
TRF2 F/- Lig4 -/- SV40
I
diplochromosomes in TRF2 F/- Lig4 -/- p53 -/- + Cre
J
POT1a F/- POT1b F/F
0 h
48 h
96 h
7%
22%
39%
bleomycin
9%
21%
41%
doxorubicin
8%
20%
UV
- OHT
+ OHT
1%
10%
TopBP1-ER
K
zeocin - + + - -
doxo - - - + +
h 0 24 48 24 48
P-Chk2
Chk2
actin
L
% polyploid cells
0 h 48 h 96 h 48 h 96 h UV
bleomycin doxorubicin
POT1a F/- POT1b F/F
M
BJ + E6E7
0 h
48 h
96 h
1%
9%
27%
zeocin
1%
8%
29%
doxorubicin
N
% polyploid cells
0 h 48 h 96 h 48 h 96 h
zeocin doxorubicin
BJ + E6E7
O
% polyploid cells
0 h 48 h 96 h zeocin
p53 -/- MEFs

Figure S1. Polyploidy Due to Persistent DNA Damage Signaling, Related to Figure 1

(A) Immunoblotting showing POT1a/b deletion and Chk1 and Chk2 phosphorylation in POT1a$^{F/-}$POT1b$^{F/F}$ MEFs after introduction of Cre.

(B) Supernumerary centrosomes in POT1a/b DKO cells. Centrosomes were detected by immunofluorescence for pericentrin in POT1a/b knockout cells and controls (no Cre). The percentage of cells containing more than two centrosomes was scored on > 50 cells for each group.

(C) Contribution of ATR to the induction of polyploidy. POT1a$^{F/-}$POT1b$^{F/F}$ MEFs were treated with ATR shRNA or vector control and polyploidy was measured by FACS after Cre expression (4 days after), zeocin treatment (48 hr after) or after no treatment. Quantification of the percentage of polyploid cells in three independent experiments and SDs are shown.

(D) Contribution of ATM to the induction of polyploidy in POT1a/b DKO cells and in zeocin-treated cells. POT1a$^{F/-}$POT1b$^{F/F}$ATM$^{-/-}$ and POT1a$^{F/-}$POT1b$^{F/F}$ ATM$^{+/-}$ MEFs were treated with Cre, zeocin, or left untreated and the percentage of polyploidy was measured by FACS. Quantification of the percentage of polyploid cells in four independent experiments with SD is shown.

(E) No effect of the ATR shRNA on the S phase index. POT1a$^{F/-}$POT1b$^{F/F}$ATM$^{-/-}$ and POT1a$^{F/-}$POT1b$^{F/F}$ATM$^{+/-}$ were treated as in Figure 1F. Cells were pulsed with BrdU for 1 hr and the percentage of BrdU positive cells was measured. Average values and SEM are shown.

(F and G) UCN01 decreases polyploidization in POT1a/b DKO cells. POT1a$^{F/-}$POT1b$^{F/F}$ MEFs were treated with Cre or vector and after 2 days were synchronized in G1/S by double thymidine block and released. Cells were pulsed for 1 hr (t = 0 hr to t = 1 hr) with BrdU in order to mark a cell population and washed. After 2 hr from release (t = 2 hr) UCN01 (2 μM) or vehicle was added and FACS was performed at the indicated time points (F). Tetraploid BrdU positive cells were gated. (G) Bargraphs showing the average percentage of tetraploid BrdU-positive cells after treatment with 2 or 5 μM UCN01.

(H) FACS analysis of TRF2$^{F/-}$Lig4$^{-/-}$ SV40 MEFs treated with Cre showing a moderate level of polyploidization after 4 days.

(I) Metaphase spread from TRF2$^{F/-}$Lig4$^{-/-}$p53$^{-/-}$ MEFs treated with Cre showing diplochromosomes. DAPI, red; Telomeric FISH, green. FISH-IF on metaphase spreads was performed as previously described (Celli and de Lange, 2005).

(J–L) Induction of polyploidy in mouse cells using various treatments to induce persistent DNA damage. POT1a$^{F/-}$POT1b$^{F/F}$ MEFs were continuously treated with the indicated drugs or with UV (20J/m^2 every 2 hr for two periods of 12 hr with 12 hr in between) and the percentage of polyploid cells was measured by FACS at the indicated time points. Alternatively, MEFs expressing TopBP1-ER were treated or not with OHT for 72 hr. Representative experiments (J) and quantification in two or more independent experiments (L) are shown. Immunoblotting showing phosphorylation of Chk2 after drug treatment at the indicated time points is shown in (K).

(M and N) Persistent DNA damage induces polyploidy in human cells. Human BJ fibroblasts expressing HPV E6 and E7 proteins were treated with the indicated drugs and polyploidy was measured by FACS at the indicated time points. Representative experiment (M) and quantification in three independent experiments (N) are shown.

(O) Absence of p53 is sufficient to allow polyploidization in MEFs. p53$^{-/-}$ MEFs were treated with zeocin and polyploidy was measured by FACS at the indicated time points. Average values from two independent experiments with SD are shown.

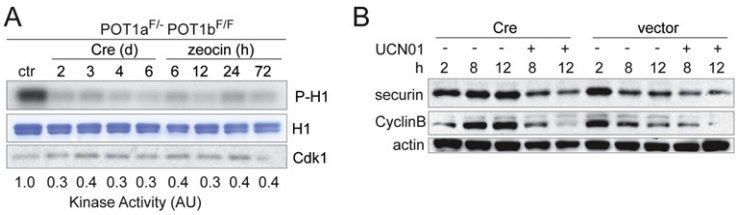

Figure S2. Impaired Activity of Cdk1/CyclinB and APC/Cdc20, Related to Figure 2

(A) Low Cdk1/CyclinB activity in POT1a/b DKO and zeocin-treated cells. POT1a$^{F/-}$POT1b$^{F/F}$ MEFs were treated with Cre or with continuous zeocin and Cdk1/CyclinB activity was measured at the indicated time points. Phopho-histone-H1, Coomassie staining of histone H1, immunoblotting showing Cdk1 and quantification of kinase activity are shown.

(B) Role of Chk1/Chk2 in stabilization of mitotic APC targets. POT1a$^{F/-}$POT1b$^{F/F}$ MEFs were treated as in Figure S1F and immunoblotting for the indicated proteins at the indicated time points is shown.

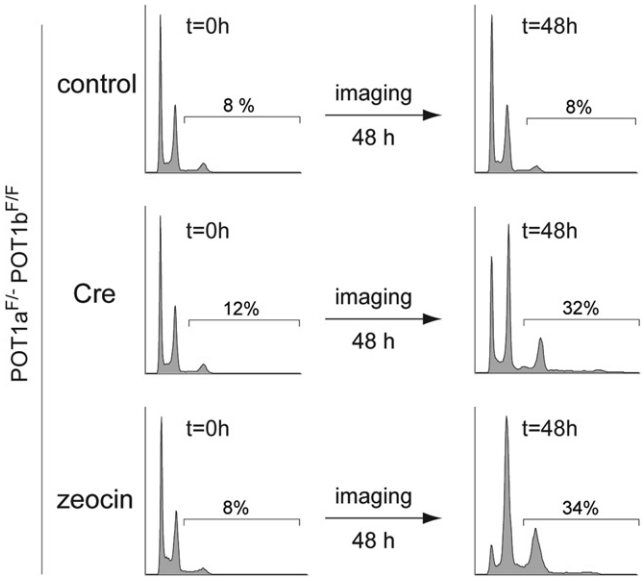

Figure S3. Polyploidization during Live-Cell Imaging, Related to Figure 3

FACS profiles of cells used in the live-cell imaging shown in Figure 3A at the beginning (t = 0 hr) and at the end (t = 48 hr) of the imaging session. Percentage of polyploid cells is shown.

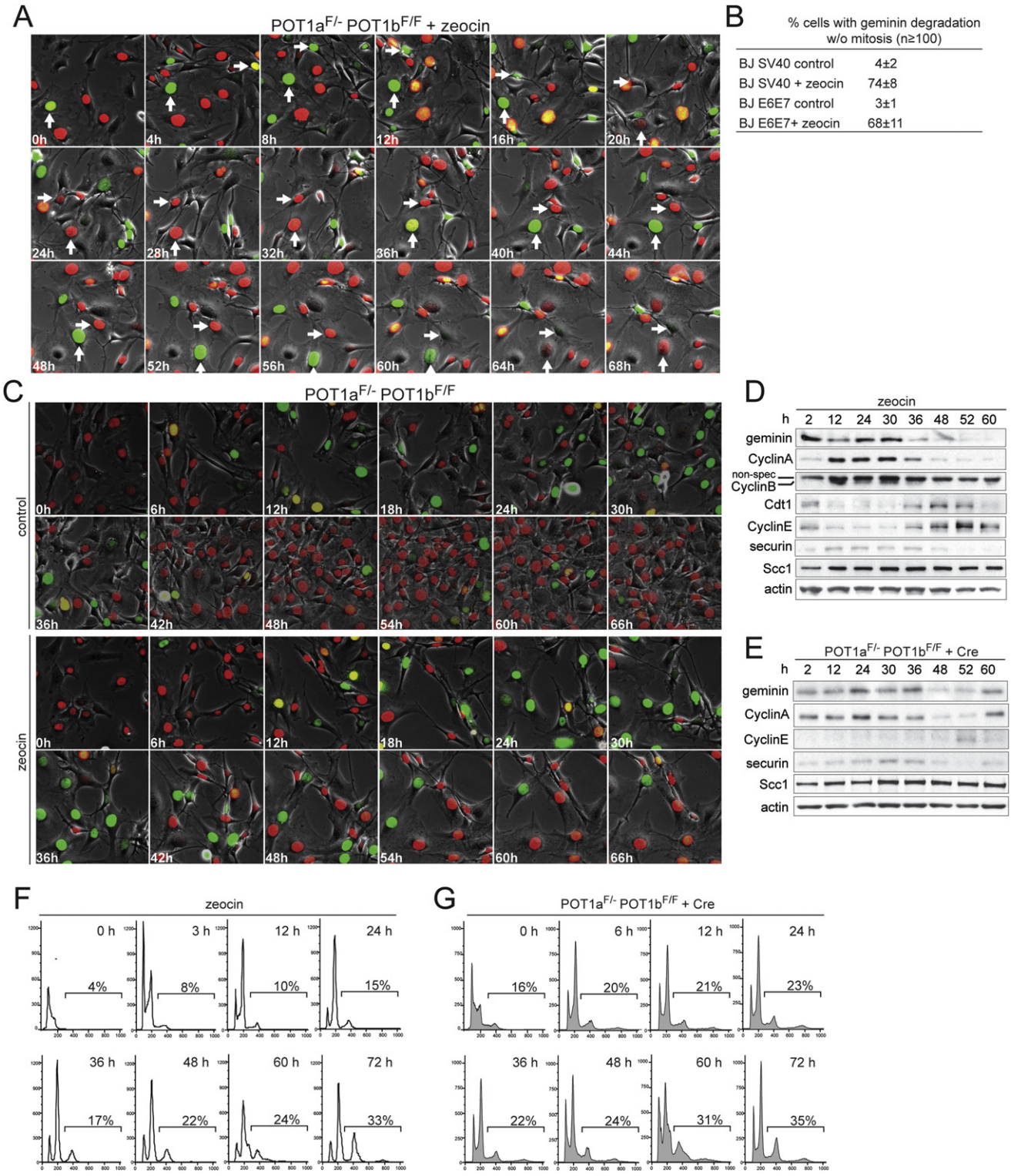

Figure S4. Fluctuations of Geminin, Cdt1, and Other Proteins in Endoreduplicating Cells, Related to Figure 4

(A) POT1a$^{F/-}$POT1b$^{F/F}$ MEFs expressing FUCCI proteins were continuously treated with zeocin and imaged as in Figure 4B (Movie S3). Selected time points are shown. Arrows with the same orientation highlight the same cell over time. Two representative cells showing geminin and Cdt1 oscillation without mitotic events are indicated.

(B) Geminin degradation in the absence of mitosis in BJ cells treated with zeocin. BJ cells expressing SV40-LT were transduced with FUCCI lentiviral vectors and imaged in the absence (control) or presence of zeocin for 96 hr (Movie S4). The percentage of cells showing at least one event of geminin degradation in the absence of mitosis during the imaging was analyzed by scoring at least 100 cells for each condition. Similar data obtained using BJ cells expressing HPV-E6/E7 are shown.

(C) FUCCI imaging of synchronized cells. POT1a$^{F/-}$POT1b$^{F/F}$ MEFs expressing FUCCI vectors were synchronized in G1 by mitotic shake-off and were imaged for 72 hr in the presence or absence of zeocin, Imaging was started 10 hr after the mitotic cells were plated. Selected time points (every 6 hr) are shown from a representative experiment. The corresponding movie is Movie S5.

(D) Analysis of the indicated cell cycle regulated proteins over time in zeocin-treated cells. POT1a$^{F/-}$POT1b$^{F/F}$ MEFs were synchronized in G1/S by double thymidine block and released in the presence of zeocin. Immunoblotting for the indicated proteins at the indicated time points is shown.

(E) Analysis of the indicated cell cycle regulated proteins in POT1a/b DKO cells. POT1a$^{F/-}$POT1b$^{F/F}$ MEFs were treated with Cre, synchronized in G1/S by double thymidine block and released. Immunoblotting for the indicated proteins are shown.

(F) FACS analysis of cells treated as in (D). FACS analysis at the indicated time points is shown and the percentage of polyploid cells is indicated.

(G) POT1a$^{F/-}$POT1b$^{F/F}$ MEFs were treated as in (E). FACS analysis at the indicated time points is shown and the percentage of polyploid cells is shown.

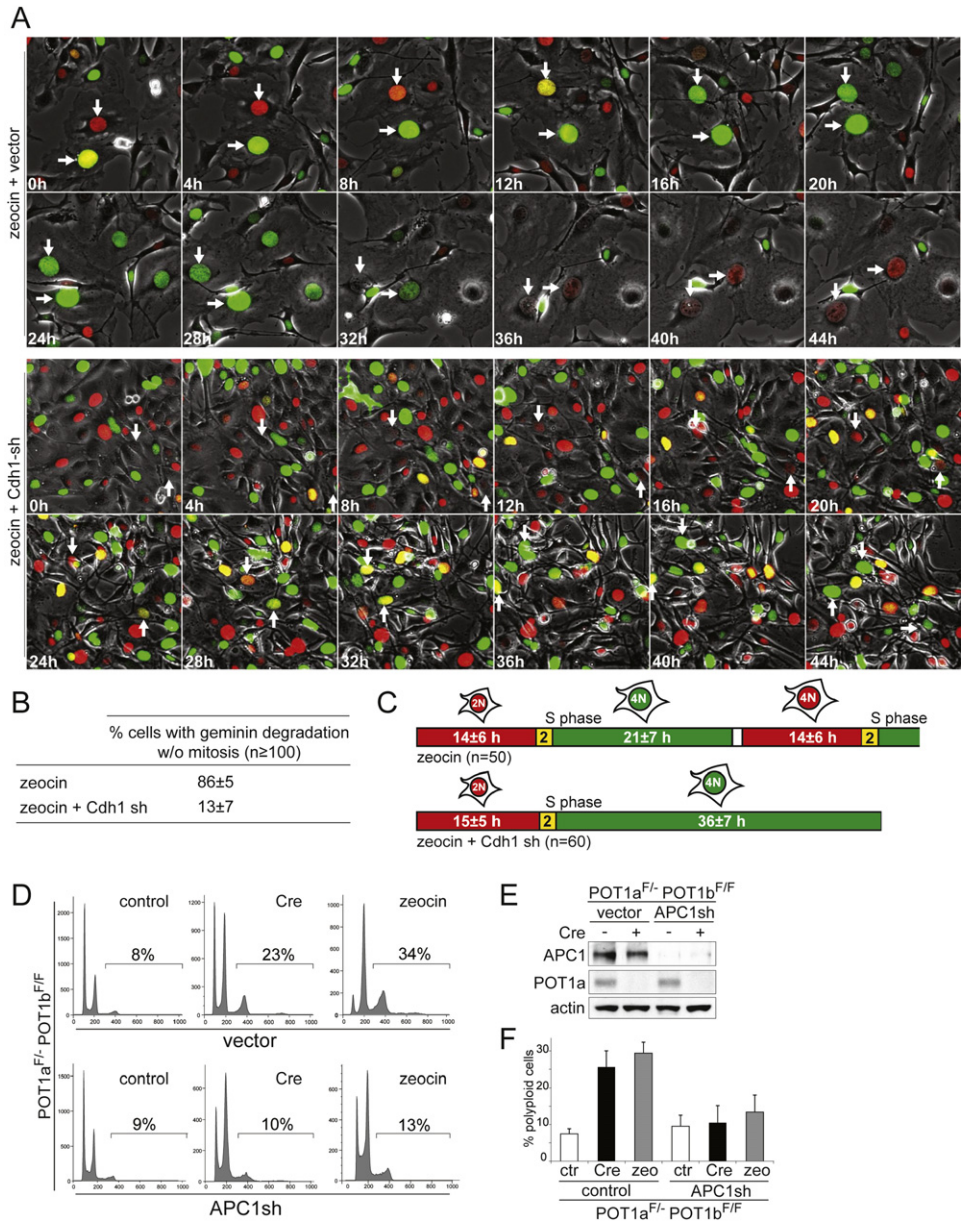

Figure S5. Involvement of Cdh1 and APC1 in Endoreduplication, Related to Figure 5

(A) Cells were treated with Cdh1 shRNA or the vector control and imaged as in Figure 5D in the presence of zeocin (Movie S7). Selected time points (every 4 hr) are shown. Arrows with the same orientation highlight the same cell during time.

(B) Table showing the effect of Cdh1 knockdown on mitosis-independent geminin degradation in zeocin-treated cells. Cells were treated and imaged as in (A). At least 100 cells were followed throughout the movie and the percentage of cells showing at least one event of geminin degradation without mitosis was determined. Average values obtained from three independent experiments with SD are shown.

(C) Diminished geminin degradation after Cdh1 knockdown in zeocin-treated cells. Cells were treated and imaged as in (A) and the indicated number of cells were followed throughout the imaging session to determine the length of G1 (red), entry into S phase (yellow), and S/G2 (green). Average values (h) are shown.

(D–F) Diminished polyploidy after knockdown of APC1. POT1a$^{F/-}$POT1b$^{F/F}$ MEFs were treated shRNA to knockdown APC (immunoblot in [E]) and polyploidy was measured after POT1a/b deletion with Cre, after continuous zeocin treatment, or in untreated cells. FACS profiles from a representative experiment (D) and quantification of the percentage of polyploid cells in three independent experiments (F) are shown.